AGU ADVANCING EARTH AND SPACE SCIENCE

Water Resources Research®

RESEARCH ARTICLE
10.1029/2021WR030058

A Multi-Inventory Ensemble Analysis of the Effects of Atmospheric Rivers on Precipitation and Streamflow in the Namgang-Dam Basin in Korea

Young Ryu[1], Hyejin Moon[1,2], Jinwon Kim[1], Tae-Jun Kim[1], Kyung-On Boo[1], Bin Guan[3], Yoichi Kamae[4], Wei Mei[5], Chanil Park[6], Seok-Woo Son[6], and Young-Hwa Byun[1]

[1]National Institute of Meteorological Sciences/Korea Meteorological Administration, Seogwipo-si, Republic of Korea, [2]National Meteorological Satellite Center, Choocheongbuk-do, Republic of Korea, [3]Joint Institute for Regional Earth System Science and Engineering (JIFRESSE)/University of California Los Angeles, Los Angeles, CA, USA, [4]Faculty of Life and Environmental Sciences, University of Tsukuba, Ibaraki, Japan, [5]Department of Marine Sciences, University of North Carolina at Chapel Hill, Chapel Hill, NC, USA, [6]School of Earth and Environmental Sciences, Seoul National University, Seoul, Republic of Korea

Key Points:

- Atmospheric river storms provide over 60% of the annual rainfall/runoff to become the primary source of water resources and extreme hydrologic events for the basin
- The seasonal cycles of runoff/runoff coefficients are primarily shaped by the seasonal cycle of soil water content in response to seasonal precipitation
- Differences among multiple atmospheric rivers (ARs) inventories are a minor concern for the uncertainties in assessing the AR effects on the hydrology in the basin

Correspondence to:
J. Kim,
jkim@atmos.ucla.edu

Citation:
Ryu, Y., Moon, H., Kim, J., Kim, T.-J., Boo, K.-O., Guan, B., et al. (2021). A multi-inventory ensemble analysis of the effects of atmospheric rivers on precipitation and streamflow in the Namgang-dam basin in Korea. *Water Resources Research*, *57*, e2021WR030058. https://doi.org/10.1029/2021WR030058

Received 7 APR 2021
Accepted 13 JUL 2021

Abstract Atmospheric rivers (ARs) are an important concern in regional water management; however, little is known about the AR impacts on hydrology in East Asia (EA). This study analyzes the characteristics of storms, precipitation (*P*), streamflow (*Q*), and runoff coefficient (*R*) in the Namgang-dam basin in Korea related to ARs for 2000–2013, as well as the sensitivity of the analysis results to AR detection methods, using observed *P*, *Q*, and three different AR inventories. The basin experiences 37.3 storms annually, of which 54% are AR storms that provide over 60% of the annual *P* and *Q*. The AR (non-AR) storms are dominant in storm frequency and the storm-total *P* and *Q* for January–July (August–December) with peaks in July (August). The monthly AR frequency varies closely with the seasonal variations in the EA monsoon and the North Pacific storm track which modulate the number of extratropical cyclones. The AR storms produce most of the extreme events; they also generate larger storm-mean *P* and *Q* than the non-AR storms for all months. The seasonal variations in *R* are related to the total (AR- and non-AR storms combined) *P* through the seasonal soil water variations, making the AR effects on *R* unclear. Considering 95% confidence intervals, the AR storms are distinguished well from the non-AR storms in storm frequency and the storm-total and storm-mean *P* and *Q*. The sensitivity to AR inventories is not critical in quantifying the AR-storm characteristics and their impacts on hydrologic variables except for *R*.

1. Introduction

Atmospheric rivers (ARs) not only play an important role in shaping the global water cycle through poleward atmospheric water-vapor transports (Guan & Waliser, 2015; Nash et al., 2018; Schneider et al., 2005; Trenberth & Stepaniak, 2003; Zhang et al., 2019; Zhu & Newell, 1998) but also critically affect the hydrology in the AR landfall regions (Guan et al., 2016; Kamae, Meix, Xie, Naoi, & Ueda, 2017; Kim et al., 2013, 2021; Ralph et al., 2004, 2006; Rutz et al., 2019; Slinskey et al., 2020). AR activities vary seasonally and geographically with the highest AR activities occurring over the mid-latitude oceans and their coastal regions where large populations and industries reside. Because of their close relationship to extreme precipitation (*P*) and streamflow (*Q*) that often cause flooding, ARs have become a key concern to water managers worldwide for water resources, flood prevention, and emergency responses (Corringham et al., 2019; Dettinger et al., 2011; Guan et al., 2010; Kamae, Meix, Xie, Naoi, & Ueda, 2017; Kim et al., 2018, 2021; Lavers & Villarini, 2013a, 2013b; Lu et al., 2013; Neiman et al., 2008; Ralph et al., 2006; Waliser & Guan, 2017; among others). Most of the existing AR studies analyzed ARs and their hydrological impacts in the west coast regions of western North America (WNA) and Western Europe (WEU) during winter (Bartusek et al., 2021; Behrangi et al., 2016; Huning et al., 2017; Kim et al., 2013, 2018; Lamjiri et al., 2017; Lavers & Villarini, 2013b; Leung & Qian, 2009; Mo et al., 2019; Neiman et al., 2008; Ralph et al., 2004; and many more as reviewed in Rutz et al., 2020). A smaller number of studies analyzed the AR effects on *Q*, primarily for WNA and WEU as well (e.g., Albano et al., 2019; Demaria et al., 2017; Dettinger et al., 2011; Guan et al., 2016; Hu et al., 2017; Ionita et al., 2020; Neiman et al., 2011; Sharma & Déry, 2020a; Young et al., 2017). Ralph

et al. (2006) showed that AR landfalls are related to all seven floods in the Russian River basin in northern California for 1997–2006. Lavers and Villarini (2013a) found that ARs are linked to the top 10 annual maximum Q in 660 US watersheds. Konrad and Dettinger (2017) found that Q is directly affected by the water-vapor flux magnitudes so that ARs play an important role in generating floods. Lavers et al. (2011) showed that ARs also affect flood risks in the United Kingdom and WEU. Paltan et al. (2017) estimated that ARs contribute to 22% of the global Q with large regional differences. AR effects on regional hydrology also depend on the season of AR activities. Demaria et al. (2017) and Sharma & Dery (2020a) found that AR-induced Q is modulated by snow in high-elevation basins in WNA because ARs mainly affect WNA in winter. In a regional modeling study, Chen et al. (2019) also showed that ARs affect Q in WNA not only by P but also by the snow and the antecedent soil water content (SWC).

Because ARs occur mostly in the warm conveyor belt of extratropical cyclones (ETCs) (Guo et al., 2020; Zhang et al., 2019), ARs are expected to affect not only WNA and WEU but also other regions during the seasons of strong ETC activities. Progresses in objective identification of ARs using gridded atmospheric data have facilitated analyzing ARs and their hydrological impacts in regions around the world other than WNA and WEU (Blamey et al., 2018; Bozkurt et al., 2021; Esfandiari & Lashkari, 2020; Gorodetskaya et al., 2014; Kamae, Mei, & Xie, et al., 2017; Kamae, Mei, Xie, Naoi, & Ueda, 2017; Kim et al., 2021; Mahoney et al., 2016; Moore et al., 2012; Massoud et al., 2020; Mundhenk et al., 2016; Park et al., 2021a; Ramos et al., 2015, 2018; Sharma & Déry, 2020b; Stohl et al., 2008; Viale et al., 2018; Ye et al., 2020). For East Asia (EA), previous studies (Kamae, Mei, Xie, Naoi, & Ueda, 2017; Kim et al., 2021; Park et al., 2021a) related the seasonal cycle of the AR frequency to the seasonal variations of the large-scale circulation and related ETC activities around Korea and EA as ETC activities over EA substantially increase in spring and early summer, the period of the northward march of the EA monsoon rainfall, then rapidly decrease from July to August (Kang et al., 2018; Kang & Son, 2021). Kamae, Mei, and Xie et al. (2017); Kamae, Mei, Xie, Naoi, and Udea. (2017); Kim et al. (2021), and Park et al. (2021a) showed that ARs affect the mid-latitude EA region, most strongly in the wet warm season from June to September, accounting for 14%–44% of P and 20%–90% of extreme P events with south Korea and Japan being the hot spots of AR-induced heavy P. Moon et al. (2019) showed that AR landfalls are related to the majority of intense summer P events in Korea. Complex terrain is known to induce large P variability (Ko et al., 2018) and rapid response of Q to P (Park & Singh, 1996) in Korea. Hence, ARs also likely affect the occurrence of high Q events in mountainous watersheds in Korea.

The methods for detecting ARs are among the key sources of uncertainties in analyzing the AR effects on regional hydrology. Currently, a number of researchers developed AR inventories based on different detection schemes, often to suit specific applications or regions (e.g., Gershunov et al., 2017; Guan & Waliser, 2015; Kamae, Mei, Xie, Naoi, & Ueda, 2017; Lavers et al., 2012; among others). A comprehensive review of a number of existing detection schemes is provided in Rutz et al. (2019). These schemes are formulated using their own unique AR-detection criteria such as shape factors and other conditions. In addition, different reanalysis data are used to derive different inventories (e.g., Guan & Waliser, 2017; Guan et al., 2018; Huning et al., 2019; Ralph et al., 2019). Wide variations in detection schemes and reanalysis data introduce differences among these inventories. From an intercomparison of over 20 AR inventories, Rutz et al. (2019) found that different AR detection schemes yield widely varying key AR characteristics such as frequency, duration, and seasonality. Because identification of the best AR detection methods and/or inventories is impossible, it is important to estimate the uncertainty due to the differences among available AR inventories in quantifying the AR characteristics and their impacts on regional hydrology (Shields et al., 2018).

Despite its importance in water resources and flood prevention, the impact of ARs on the P and Q in EA and Korea remains largely unexplored. Despite a few studies analyzed ARs and their impacts on P in EA, the relationship between ARs and basin-scale Q in EA has not been explored. This study analyzes the climatology of the AR-related P and Q in the Namgang-dam basin, an unmanaged headwater of the Nackdong-river which is the second largest river in Korea with a history of frequent flooding (Kim et al., 2020; Ryu et al., 2017). Because the basin and its downstream regions support large populations and industries, the effects of ARs on P and Q in the basin are of great concern in water management for water resources and flood prevention. This paper is organized as follows. Section 2 presents the experiment and the AR

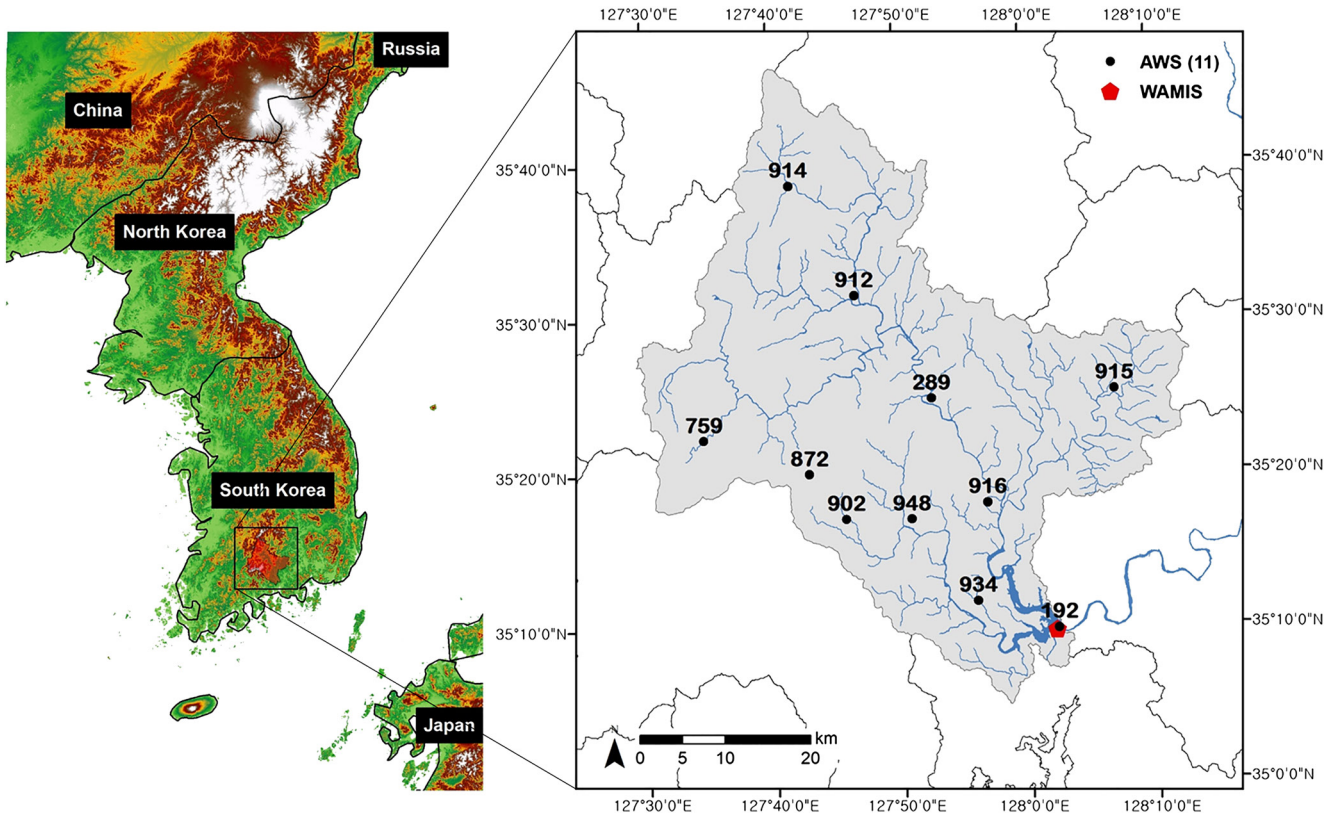

Figure 1. The location of the Namgang-dam basin in Korea (the red area in the box on the left). The blue lines indicate the channels within the basin. The black dots and the red dot in the right-hand side figure are the locations of automatic weather stations and hydrograph, respectively, within the Namgang-dam basin.

inventories and observed data employed in this study. Section 3 presents the results from the analyses and Section 4 summarizes the results and provides additional discussions.

2. Site, Materials, and Methods

The Namgang-dam basin covers an area of 2,281.7 km^2 with a mean elevation of 247.6 m above sea level (Figure 1). The Special Sensor Microwave Imager/Sounder precipitable water vapor image, vertically integrated water vapor transport (IVT), and the AR locations depicted in the three inventories used in this study on June 18, 2013, are shown in Figure 2 for an example of an AR that affected the basin. The basin receives an annual-mean P of 1,584.2 mm, about 1.2 times of the annual-mean P in Korea (1,274 mm), most of it in summer and early fall (June–September) when the region is affected by the EA monsoon, tropical cyclones (TCs) and thunderstorms (TSs). The climatological annual Q in the basin is 0.102 mm h^{-1} (893.5 mm year^{-1}) with the peak flow and the standard deviation of 12.4 and 7.8 mm h^{-1}, respectively. All peak flow events occurred in summer except during the three strong TCs in the September of 2003 (typhoon MAEMI), 2007 (typhoon NARI), and 2011 (typhoon SANBA). The basin is natural, that is, not artificially controlled by dams, levees, and/or aqueducts.

Hourly P at 11 automatic weather stations (AWSs) of Korea Meteorological Administration (black circles in Figure 1) in the basin (available at: data.kma.go.kr) and the hourly Q at the Namgang-dam inlet point (red square in Figure 1) from the Water Resources Management Information System (WAMIS: available at www.wamis.go.kr) are used in this study. The analysis covers the 14-year period 2000–2013, the maximum overlapping period of the three AR inventories employed in this study. Quality control of the P and Q data is performed by KMA and WAMIS, respectively. The basin-mean P is calculated from the AWS data using the Thiessen method; the results using the basin-mean P from simple averaging of the AWS data are essentially

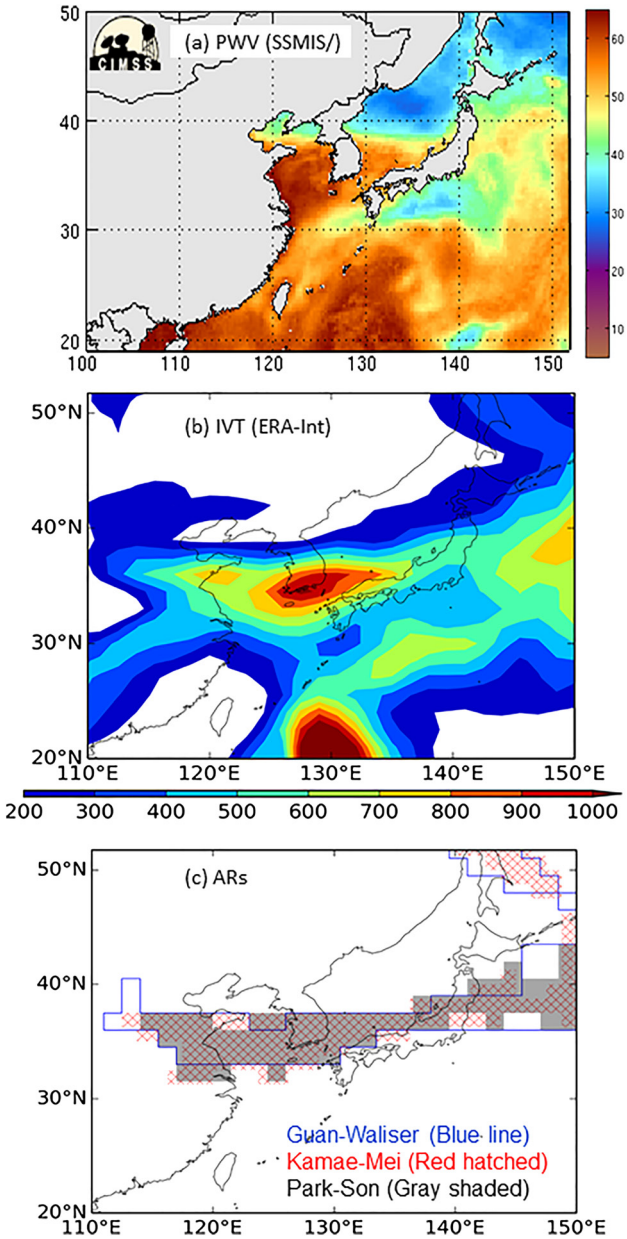

Figure 2. An atmospheric river (AR) landfall in southern Korea coast at 00UTC on June 18, 2013: (a) Precipitable water vapor (from ftp://ftp.ssec.wisc.edu/pub/mimic-tpw/images/wpac/), (b) Vertically integrated water vapor transport in the ERA-Interim reanalysis, and (c) The corresponding AR shapes in the three inventories.

identical to those reported in this study. For a more intuitive comparison between P and Q, the Q values are converted from $m^3\ s^{-1}$ to mm h^{-1}, the units of P, by dividing the Q values (originally in $m^3\ s^{-1}$) by the basin area (in m^2) and with appropriate unit conversions.

Unlike most of the previous studies that analyzed ARs and their effects based on the instantaneous relationship between the presence of AR and P at fixed time intervals, either daily or 6-h (e.g., Dettinger et al., 2011; Kamae, Mei, & Xie, 2017; Kim et al., 2013, 2018, 2021; Neiman et al., 2008; Ralph et al., 2006; and many more), this study analyzes P and Q on the basis of storm events (e.g., Chen et al., 2019; Lamjiri et al., 2017) to better capture the time- and basin-integrated effects of P on Q. The storm-based analysis is directly applicable to water management operations for planning and designing storm-water handling structures for protecting the human society and environments (Adams et al., 1986; Guo, 2001; Guo & Adams, 1998; Guo & Baetz, 2007). In order to match the 6-h AR inventories, storms are identified following Lamjiri et al. (2017) using the 6-h P time series constructed by summing 6 h P values around the corresponding AR detection time. A matching 6-h Q time series is constructed using the hourly Q in the same way. A storm is defined as an event of consecutive 6-h periods of non-zero P over which more than 5 mm of P is accumulated. A storm is tagged as an AR storm if ARs occur over the basin for at least half of the storm period; if not, it is tagged as a non-AR storm. Varying the threshold AR occurrence between 50% and 70% yields practically the same results as reported in this study. The characteristics of AR and related P and Q analyzed in this study are presented in Table 1.

For a multi-inventory ensemble analysis, this study employs three AR inventories from Guan and Waliser (2015), Kamae, Mei, Xie, Naoi, and Ueda (2017), and Park et al. (2021a) (hereafter referred to GW, KM, and PS, respectively) to estimate the uncertainty in the analysis results related to the differences among multiple AR inventories. The three AR inventories are constructed by applying detection schemes based on IVT at 6-h intervals using the European Center for Medium-Range Weather Forecasts global reanalysis ERA5 (Hersbach et al., 2020) for PS, the ERA-interim reanalysis (Dee et al., 2011) for GW and the JRA-55 reanalysis (Kobayashi et al., 2015) for KM. These three AR inventories have been used in a number of AR studies, from the global water-vapor transports to AR-related regional hydrology (Guan & Waliser, 2015; Espinoza et al., 2018; Kamae, Mei, Xie, Naoi, & Ueda, 2017; Kamae, Mei, & Xie, 2017; Kim et al., 2018; Park et al., 2021a; Waliser & Guan, 2017). Details of the AR detection method and its evaluation are referred to Guan and Waliser (2015), Kamae, Mei, Xie, Naoi, and Udea (2017), and Park et al. (2021a). Note that intercomparison and/or evaluation of these AR inventories and associated detection methods are not a subject of this study. A comprehensive intercomparison of a large number of AR detection schemes is currently carried out in community efforts such as the Atmospheric River Tracking Method Intercomparison Project (Shields et al., 2018). The multi-inventory ensemble approach based on storm events using observed P and Q is unique among the existing studies on the AR effects on regional hydrology, not only for EA but also for other regions around the world.

The 95% confidence interval based on the Student's t-test is used to assess the separation of the ensemble-mean properties related to the AR storms from the non-AR storms. Note that only the AR and non-AR storms vary according to inventories because storms are defined solely by P and, thus, the mean properties of all (AR and non-AR combined) storms are independent of AR inventories. Because only three inventories

Table 1
Definition of Precipitation and Runoff Characteristics

Variable name	Definition	Units
Storm	A consecutive period of 6-h intervals with non-zero P with over 5 mm accumulated P. A storm is separated from its neighboring storms by a dry period of one or more 6-h intervals.	–
Storm frequency	The number of storms in a month	$month^{-1}$
Storm duration	The period from the start to the end of each storm.	h
Storm-mean duration	The average duration of storms	h $storm^{-1}$
Storm-total precipitation	The sum of P over all storm events.	mm
Storm-mean precipitation	Storm total P divided by the number of storms	mm $storm^{-1}$
Storm-total runoff	The sum of Q over all storm events	mm
Storm-mean runoff	Storm total Q divided by the number of storms	mm $storm^{-1}$
Runoff coefficient	Q divided by P ($R = 100^*Q/P$)	%

are used in the analyses, the uncertainties due to the differences between the inventories may not be meaningfully measured in terms of conventional estimates such as signal-to-noise ratio (Kim et al., 2015) or inter-member variance. This study defines a simple uncertainty measure the "uncertainty range" (UR) as the difference between the maximum and minimum values obtained by applying individual inventories (i.e., three AR inventories yield three different values) to measure the uncertainty due to the differences between the inventories. UR is used in conjunction with the 95% confidence interval of ensemble means as a rough estimate for if the differences between the inventories are an important concern in the analyses; if UR is within the 95% confidence interval, the differences between the inventories are not likely a concern at the 95% significance level.

3. Results

This section analyzes the climatology of the storm properties and related P, Q, and the runoff coefficient ($R = 100^*Q/P$ (%)) (Table 1) in terms of their association with ARs. These variables are directly related to water resources and potential flood risks that are among the key concerns in water management such as designing the flood-control infrastructure (Castro et al., 1999; Cerdan et al., 2004; Chandimala & Zubair, 2007; Conway et al., 2009; Gottschalk & Weingartner, 1998; López-Moreno et al., 2007; Sherman, 1932; Sivapalan et al., 2005; Trigo et al., 2004).

3.1. Storm Frequency and Duration

An average of 37.3 storms $year^{-1}$ have occurred over the Namgang-dam basin during the 14-year period; among them, 54% are AR storms. Frequencies of both the AR- and non-AR storms undergo clear seasonal cycles (Figure 3a). The AR-storm frequency peaks in July and exceeds the non-AR storm frequency from February to July while the non-AR storm frequency peaks in August and exceeds the AR storm frequency from August to January. The seasonal variations in the AR- and non-AR storm frequency are likely related to the seasonal cycle of the large-scale circulation over EA as discussed in Section 4. The weak AR storm activities from October to January are related to weak ETC activities and small atmospheric water vapor contents during the dry period. The monthly mean AR storm frequency is well outside the UR of the non-AR storms except for February. Thus, the storm frequency difference between the AR and non-AR storms is beyond the uncertainty related to the differences among the three AR inventories.

The annual-mean AR storm duration (33.2 h) is nearly the same as the non-AR storm duration (34.0 h) considering that the storm-detection time step is 6 h. The monthly AR storm-mean durations are well outside the 95% significant range of their neighbors except during the dry period, October–January, with a clear single-peak in August while most of the non-AR storm-mean durations are within the 95% confidence interval of their neighboring months without clear peaks (Figures 3b and 3c). That is, the AR storms go through a well-defined annual cycle while the non-AR storms do not. For both the AR and non-AR storms,

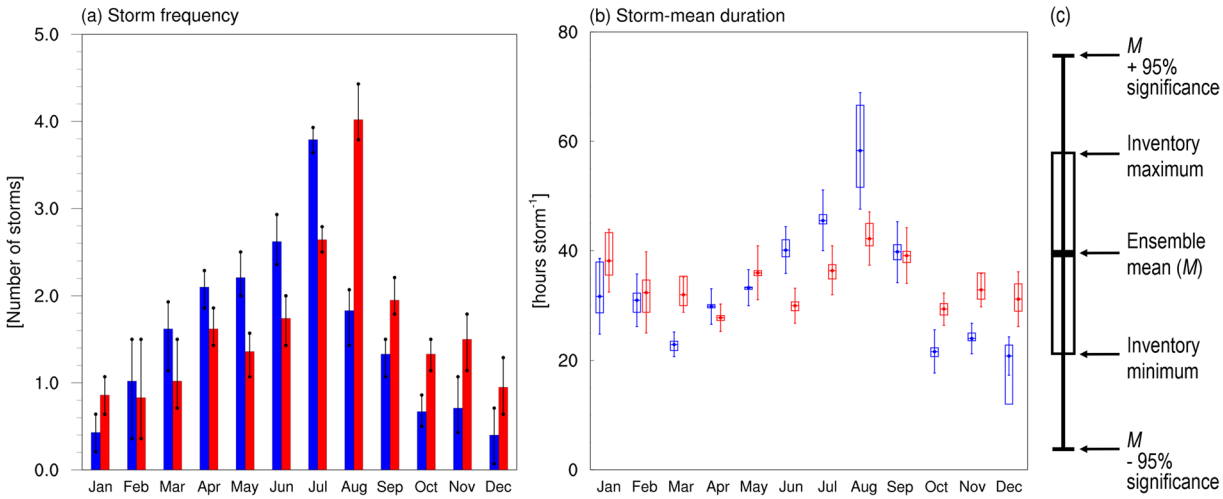

Figure 3. The (a) Storm frequency and (b) Storm-mean duration of the atmospheric river (AR) (blue) and non-AR (red) storms. The bars in (a) indicates the range of the minimum and maximum values in the estimates for individual inventories. (c) The box-whisker diagrams in (b) present the ensemble mean value (the cross bar within a box), the minimum and maximum values based on individual inventories (the bottom and top of a box), and the 95% confidence interval based on Student's *t*-tests (the whisker).

the uncertainty in the storm-mean duration due to the differences between the inventories (UR is indicated by the top and bottom end of each box, respectively, see Figure 2c) are within the 95% confidence interval except for the AR storms in December. Hence, the differences between the inventories are not likely critical for estimating the storm-mean durations for both the AR and non-AR storms.

3.2. Storm Precipitation

The all-storm P in the basin (gray bars in Figure 4a) undergoes an annual cycle with the peak in July (373.2 mm month^{-1}) and August (374.6 mm month^{-1}). The AR storms (604.7 mm) bring 64% of the summer (June–August) P total (939.8 mm) and 61% (972.8 mm) of the annual P total (1,585.1 mm). Thus, the AR storms contribute to the summer and the annual P is nearly twice as much as the non-AR storms. The AR and non-AR storm-total P also shows seasonal cycles with the maximum in July (277.9 mm month^{-1}) and

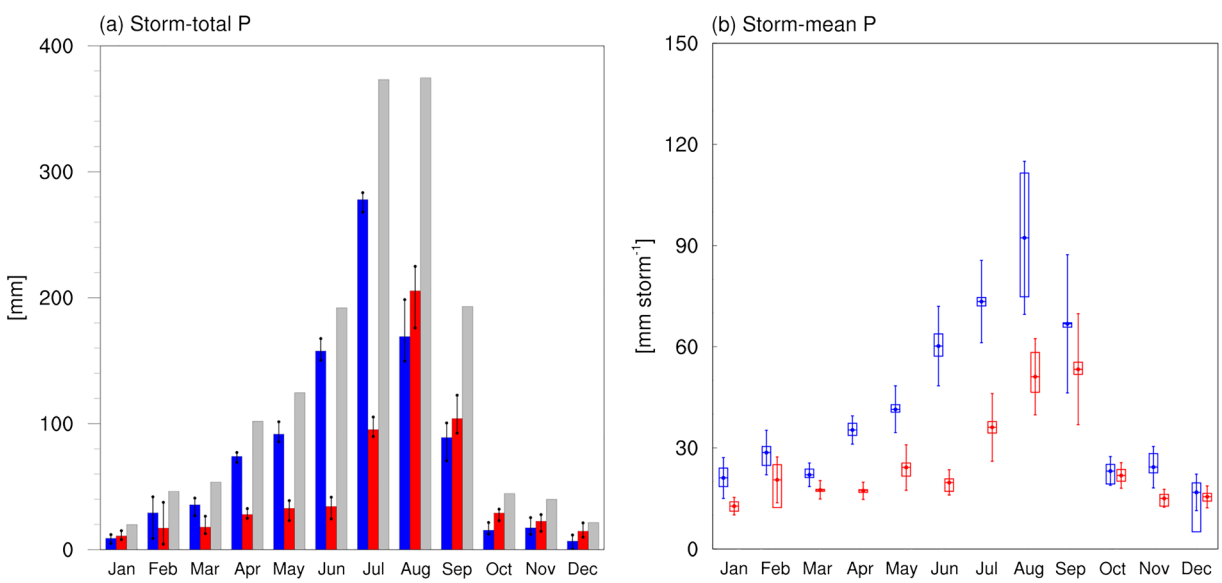

Figure 4. The monthly (a) Storm-total P and (b) Storm-mean P of the atmospheric river (AR) (blue) and the non-AR (red) storms. Gray bars in (a) are the monthly P for all (AR and non-AR) storms. See Figure 3c for the storm properties represented in the box-whisker plot in (b).

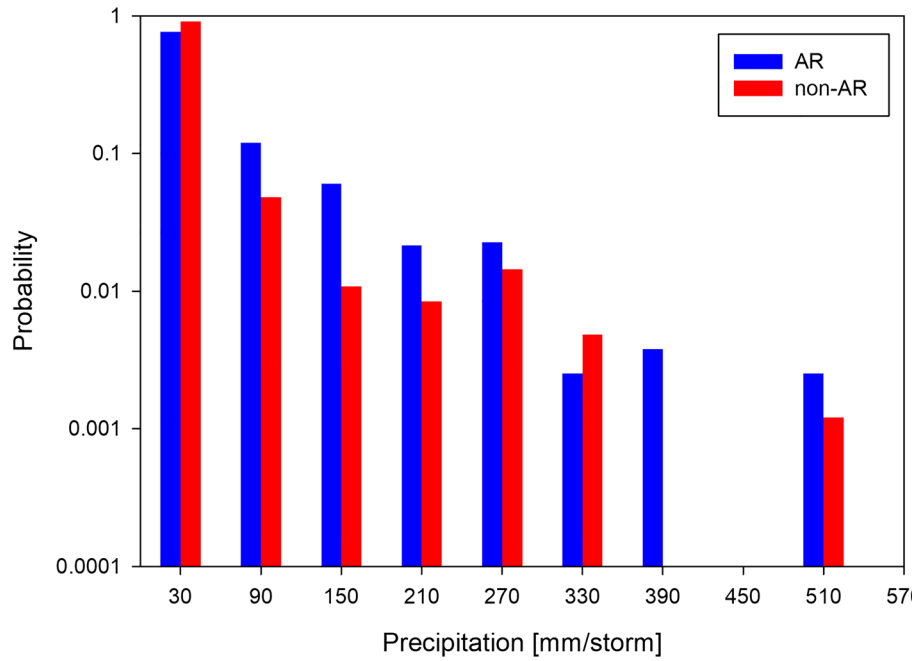

Figure 5. The probability distribution function of *P* during individual storms.

August (205.5 mm month^{-1}), respectively. The AR storms produce more *P* than the non-AR storms in spring and early summer while the non-AR storms generate more *P* from August to January. The contribution of the AR storms to the monthly *P* is especially large from May to July when Korea is affected by the ETCs associated with the EA monsoon (Kamae, Mei, Xie, Naoi, & Ueda, 2017; Kim et al., 2021; Park et al., 2021a). August and September in which the non-AR *P* exceeds the AR *P*, are strongly affected by TCs and TSs that do not typically accompany ARs. In the dry period October–January, the North Pacific storm track migrates eastward, resulting in weak AR contributions to *P*. The monthly *P* is clearly separated between the AR and the non-AR storms from March to September (the non-AR *P* is outside the UR of the AR *P*, and vice versa); the separation is not clear (the monthly non-AR *P* is within the UR of the monthly AR *P*) during the dry period (October-January) when the non-AR storms provide the majority of the monthly *P*, albeit small (Figure 4a). The differences between the AR and non-AR storm *P* are well outside the UR of both AR and non-AR storm *P*. Hence, the differences between the three inventories do not appear to be critical in estimating the AR effects in the monthly *P*, especially for the wet months.

The storm-mean *P* (Figure 4b) also undergoes similar seasonal variations as the storm-total *P* (Figure 4a) with the peak in August and September for the AR and non-AR storms, respectively; however, unlike the storm-total *P* in Figure 4a, the AR storm-mean *P* (blue) exceeds the non-AR storm-mean *P* (red) throughout the year. The AR storm-mean *P* is clearly separated from the non-AR storm-mean *P* (i.e., the storm-mean AR *P* is outside the 95% confidence interval of the non-AR storm-mean *P*) except in September, October and December; the separation is especially prominent for April-August. In addition, the UR of the storm-mean *P* is within the 95% confidence interval for both the AR and non-AR storms in all months. Thus, the uncertainty due to the differences between the inventories is expected to be small in estimating the storm-mean *P* for both the AR and non-AR storms.

Figures 3 and 4 show that the peak monthly non-AR *P* in August (Figure 4a) results from the highest non-AR storm frequency (Figure 3a) and strongest (i.e., storm-mean *P*) non-AR storms (Figure 4b) in the same month; however, the maximum storm frequency and the storm-mean *P* occur in different months for the AR storms. The monthly AR storm *P* (Figure 4a) peaks in July when the AR storms are most frequent (Figure 3a) but the AR storm-mean *P* is the second largest (Figure 4b).

The probability distribution function (PDF) of *P* for individual storms (Figure 5) shows that the non-AR storms outnumber the AR storms in the lightest *P* range, 30 mm storm^{-1} or smaller. Above this range, the

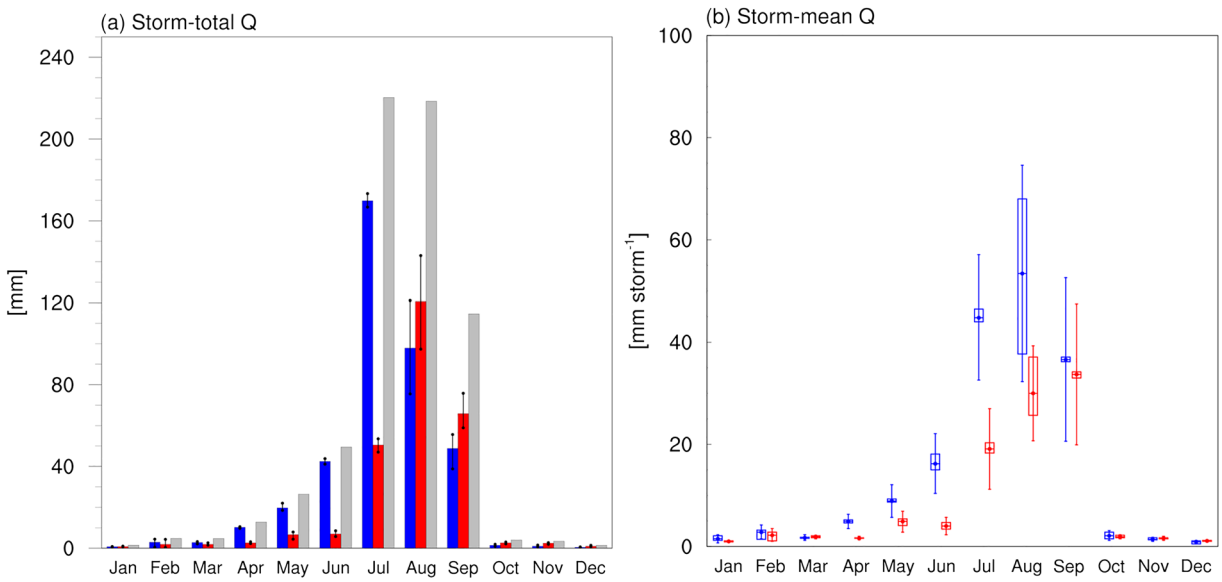

Figure 6. The monthly (a) Storm-total Q and (b) Storm-mean Q of the atmospheric river (AR) (blue) and non-AR (red) storms. Gray bars in (a) are the monthly Q for all storms. See Figure 3c for the storm properties represented in the box-whisker plot in (b).

AR storms are generally more frequent than the non-AR storms; AR storms notably outnumber non-AR storms in the range over 390 mm storm^{-1}. Because most of the storms in the heaviest P range are the AR storms, the AR storms can induce higher flood potential than the non-AR storms as pointed out in earlier studies (Hirota et al., 2016; Kamae, Mei, & Xie, 2017; Kamae, Mei, Xie, Naoi, & Ueda, 2017; Kim et al., 2021; Manda et al., 2014; Park et al., 2021a).

3.3. Streamflow

The annual all-storm (AR and non-AR combined) total Q in the basin is 661.9 mm, of which 74% (488.3 mm) occurs in summer, June–August. The AR storms contribute to 60% (64%) of the annual (summer) Q, similarly, as for P. Thus, the AR storms are the major source of water resources in the basin. The annual cycle of the all-storm total Q (gray bars in Figure 6a) is in-phase with the all-storm total P (gray bars in Figure 4a) with peaks in July (220.3 mm) and August (218.5 mm), the two months of the largest all-storm total P. The maximum AR storm-total Q occurs in July (169.8 mm) while the non-AR storm-total Q peaks (120.6 mm) in August. The annual cycles of the AR and non-AR storm-total Q are in-phase with the corresponding P, implying that the monthly Q is mainly determined by the corresponding P. For summer, the AR storm-total Q (310.2 mm) is nearly twice of the non-AR storm-total Q (178.1 mm); annually, the AR storm-total Q (398.1 mm) is 1.5 times of the non-AR storm-total Q (263.7 mm). It is also noted that the monthly storm-total Q deviates noticeably from the monthly storm-total P in the wettest period of the year, June–September. While the monthly all-storm total P (the gray bars in Figure 4a) in the period is nearly symmetric around the two wettest months (July–August), the all-storm total Q varies asymmetrically (gray bars in Figure 6a) with substantially larger Q in September than in June despite the similar amount of all-storm P in the two months. Potential causes of this difference in the annual cycle between P and Q are discussed in Section 4. The monthly AR storm-total Q exceeds the non-AR storm-total Q in all months except August and September when the non-AR-storm P exceeds the AR-storm P. The AR storm-total Q is clearly separated from the non-AR storm-total Q from March to September beyond the uncertainty related to the inventory differences as the ensemble means of the AR storm-total Q are well outside the UR of the non-AR storm-total Q of the same month. The AR storm-total Q is also outside the UR of the non-AR storm-total Q except for August (Figure 6a). Although the AR storm-total Q is not clearly separated from the non-AR storm-total Q for October-March, this may not be a critical concern because Q is small in the dry period. Thus, the uncertainty due to the differences between the inventories is not likely critical in quantifying the contribution of ARs to Q and related concerns such as the occurrence of natural disasters and water resources in the basin.

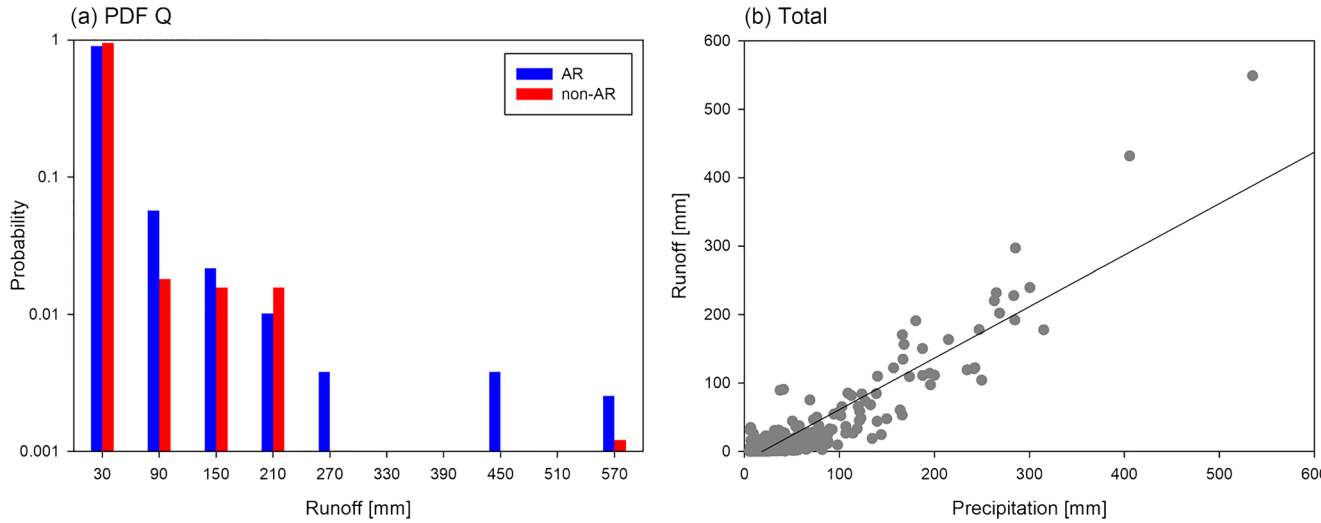

Figure 7. The (a) Probability distribution function of *Q* during individual storms and (b) The *P*-*Q* relationship for all (atmospheric river [AR] and non-AR combined) storms.

The storm-mean *Q* undergoes a clear annual cycle (Figure 6b) as the storm-mean *P* (Figure 4b). The AR storm-mean *Q* exceeds the non-AR storm-mean *Q* in all months (Figure 6b) although the non-AR storm-total *Q* exceeds the AR storm-total *Q* in August and September (Figure 6a). Hence, the large non-AR storm-total *Q* in August and September is due to a large number of non-AR storms in the two months (Figure 3a). During summer, the AR storm-mean *Q* is over twice the non-AR storm-mean *Q*. Hence, the AR storms produce, on average, more intense *Q* events and higher flood potential than the non-AR storms. The non-AR storm-mean *Q* is largest (33.7 mm storm^{-1}) in September, similarly, as for the storm-mean *P*. This suggests that, for individual storms, the amount of *P* mainly determines the amount of *Q*. Considering the 95% confidence interval, the effects of ARs on the storm-mean *Q* is well identified (i.e., the AR storm-mean *Q* are outside the 95% confidence interval of the non-AR storm-mean *Q*) for most of the wet months except September. The uncertainty due to the differences among the three inventories is also small as the UR of the AR storm-mean *Q* is well within the 95% confidence interval for almost all months, especially during the wet period.

Association of the AR storms with intense *P* events and its consequence on *Q* in the basin are clearly demonstrated by the PDF of *Q* (Figure 7a). As the PDF of *P* (Figure 5), the non-AR storms are more frequent in the range below 30 mm storm^{-1} while the ranges above 30 mm storm^{-1} are generally dominated by the AR storms. Four out of the five *Q* events that exceed 240 mm storm^{-1} are related to the AR storms. For individual storms, *Q* is well correlated with *P*, especially in the heavy *P* range over 100 mm storm^{-1} (Figure 7b). The PDF of *Q* (Figure 7a) and the *P*-*Q* relationship (Figure 7b) show that nearly the entire *P* is converted into *Q* resulting in high flood potential during intense storms.

3.4. Streamflow Response to Precipitation

This section analyzes *R* which varies following the characteristics of basin geography and *P* (Rodríguez-Blanco et al., 2012; von Freyberg et al., 2018) and has been used in regional hydrology studies to measure the response of *Q* to *P* during storms, especially for flood frequencies. The annual *R* from the all-storm *Q* and *P* is 42% which is within the range estimated in previous studies (e.g., $1\% < R < 50\%$ for cultivated basins Critchley, 2013; $R \approx 35\%$ for basins prone to flash floods Marchi et al., 2010).

The monthly *R* calculated from the all-storm *Q* and *P* increases from January to September with peaks in the three wettest months July-September when *R* is nearly 60%, then collapses suddenly in October and remains small for the rest of the year. The annual cycle of the all-storm *R* resembles that of *Q* (Figure 6a) which also shows maxima from July to September, then becomes very small in October. The monthly AR and non-AR storm-total *R* also vary similarly to the all-storm *R* (Figure 8a). The AR-storm total *R* is comparable to the

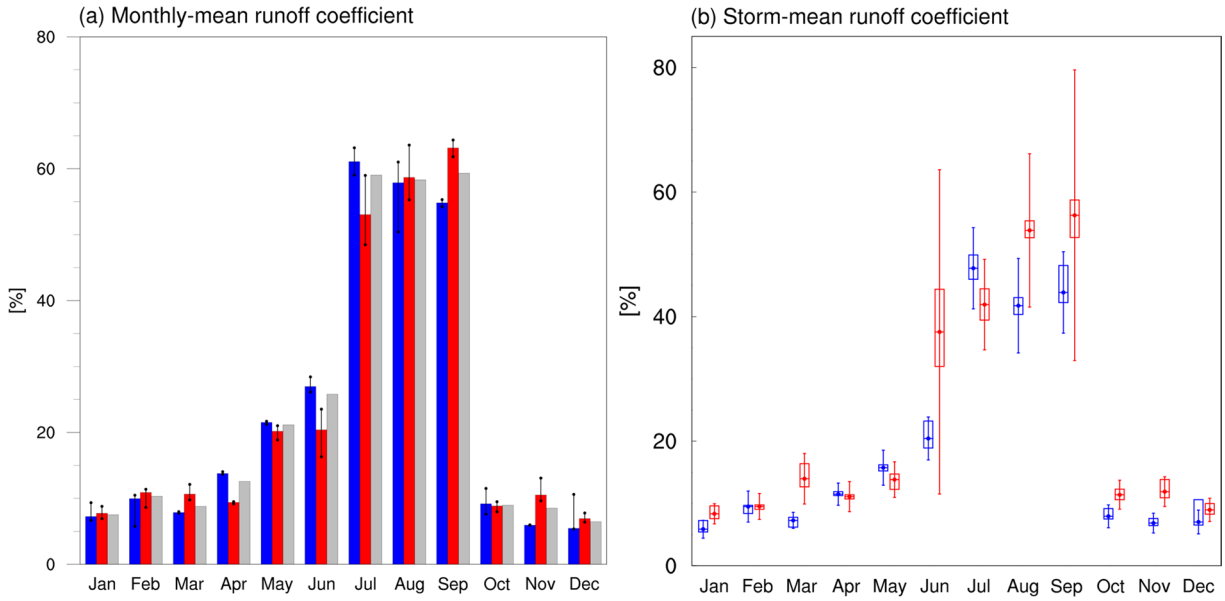

Figure 8. The annual cycle of runoff coefficient (*R*): The blue, red, and gray bar indicates the R for the atmospheric river (AR), non-AR, and all storms. See Figure 3c for the storm properties represented in the box-whisker plot in (b).

non-AR-storm total *R* for all months despite large differences in *P* and *Q*. For example, the AR storm-total *P* and *Q* are over twice the non-AR storm-total *P* and *Q* from February to July, but the differences in *R* between the AR and non-AR storms are well below 10%. Thus, when the monthly total is concerned, ARs affect *R* only slightly. Although the non-AR storm-total *R* is outside the UR of the AR storm-total *R* for most months, the separation between the AR and non-AR storm *R* is much smaller than that for *P* and *Q*. Thus, unlike for *P* and *Q*, the differences between the AR inventories may not be ignored in estimating the AR effects on *R*. The annual cycle of *R* in Figure 8a also follows closely that of the all-storm total *P* (Figure 4a) except that *P* decreases sharply from August to September while *R* remains similar for the all, AR, and non-AR storm totals. It is also noted that while *P* in June is similar to *P* in September (Figure 4a), *R* is substantially larger in September than in June (Figure 8a). This implies that *R* is controlled not only by *P* but also by some basin-specific parameters. This is further discussed in Section 4.

The storm-mean *R* (Figure 8b) shows a similar annual cycle as the storm-total *R* (Figure 8a). Unlike the storm-mean *P* and *Q*, the AR storm-mean *R* are not well separated from the non-AR storm-mean *R* as the AR storm-mean *R* is within the 95% confidence interval (whiskers in Figure 8b) of the non-AR storm-mean *R* except for several dry months. Considering that the storm-mean *P* and *Q* are well separated between the AR and non-AR storms in most months, this suggests that some factors other than *P* also affect *R* as discussed in the following section. The differences between the AR inventories may not be critical in calculating the AR effects on the storm-mean *R*, however, as the UR is well within the 95% confidence interval for all months but December and January despite the weak separation of the AR-storm means from the non-AR storm means.

The AR-storms also show similar *R* PDF as the non-AR storms (Figure 9a). For both the AR and non-AR storms, the PDF decreases until *R* reaches the 80%–90% range, then increases substantially in the range >90%. The *P*-*R* relationship in Figure 9b indicates that a number of large *R* events occur not only during strong storms but also during weak storms ($P < 10$ mm storm^{-1}). The large *R* during the storms of small *P* may occur when the baseflow and/or *Q* from preceding storms exceed *P*. The large *R* events during the storms of small *P* are more frequent for the non-AR storms than for the AR storms (not shown).

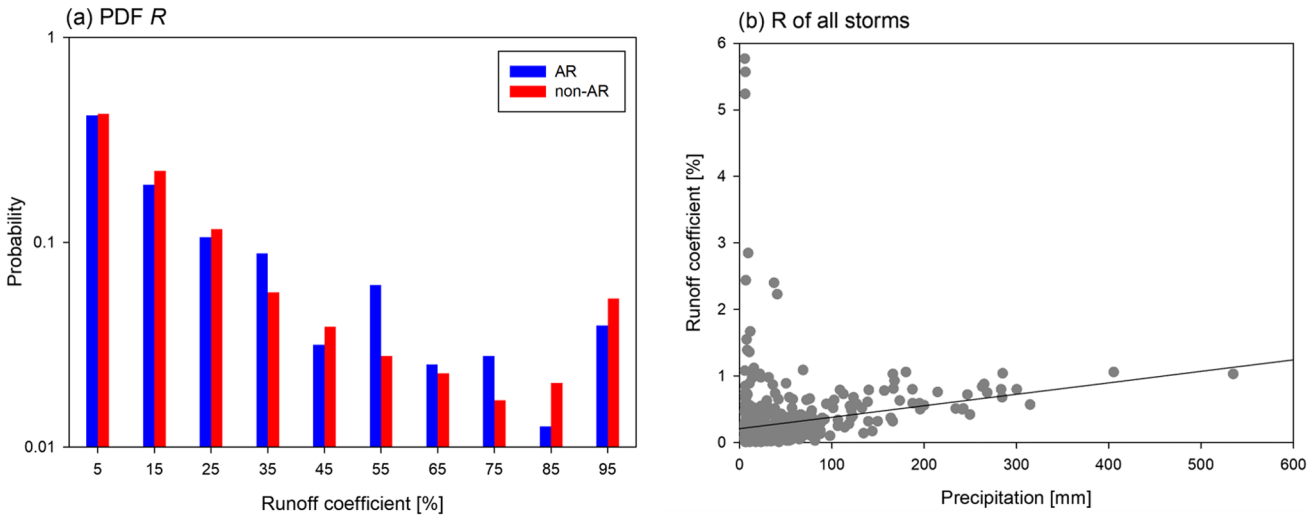

Figure 9. The (a) Probability distribution function of *R* during individual storms and (b) The *P*-*R* relationship for all storms.

4. Summary and Discussions

ARs in EA have become a topic of intense research as recent studies revealed their effects on *P* in the region, especially the occurrence of extreme *P* events in EA. Hence, quantifying the AR effects on extreme *P* and *Q* in major river basins is critical to regional water management efforts. This study analyzes the climatology of the AR effects on *P*, *Q*, and *R* in the Namgang-dam basin in southern Korea during the 14-year period 2000–2013 using observed *P* and *Q* data. Three 6-h AR inventories are used to identify the AR storms affecting the basin in order to estimate the uncertainty in quantifying the AR effects on the regional hydrology due to the differences between AR inventories. The analyses are based on storm events instead of the more conventional instantaneous AR-*P* (*Q*) relationship used in most of the previous studies to take into account the fact that the time- and basin-integrated *P* determines the *Q* at the basin outlet point. The use of multiple inventories and observed *P* and *Q* in conjunction with storm-based analyses make this study unique among the existing AR studies.

The frequency of the AR and non-AR storms undergoes a clear annual cycle with peaks in July and August, respectively. The AR storms account for 54% of storms annually and outnumber the non-AR storms in the early part of the year (February-August) while the non-AR storms are more frequent in the latter part of the year (September–January). The annual cycle of AR-storm frequency is thought to be related to the seasonal cycle of the large-scale circulation and related ETC activities around Korea and EA (Kamae, Mei, Xie, Naoi, & Ueda, 2017; Kang & Son, 2021; Kim et al., 2021; Park et al., 2021a) because over 80% of ARs are accompanied by ETCs (Zhang et al., 2019). The increase in AR frequencies and ETCs in late spring and early summer can be related to the northward movement of the EA monsoon as moist processes are critical in developing ETCs around Korea (Kang et al., 2018; Park et al., 2021b). The dominance of the non-AR storms over the AR storms in late summer and fall are related to TCs and TSs, typical non-AR storms that often produce heavy rainfall, in conjunction with weakened ETC activities over EA due to eastward migration of the North Pacific storm track from late summer. The differences between the AR inventories are not likely a serious problem in estimating the AR and non-AR storm frequencies. The annual-mean AR storm duration is essentially the same as the non-AR storm duration. The AR storm duration undergoes a clear annual cycle with the peak in August, while the non-AR storm durations do not exhibit a clear annual cycle. The key features of the annual cycle of the AR storm duration, winter minima, and summer maxima, may be related to the findings in Guan and Waliser (2019) that AR travels slower in summer than in winter due to weaker background mid-latitude westerlies (their Figure 14). As an AR travels slower, it can stay over a region longer. Considering the 95% confidence interval only the AR storms exhibit a clear seasonal cycle in the storm-mean durations.

The AR storms generate the majority of *P* in the basin: 61% for annually and 64% in summer. The AR (non-AR) storm *P* shows clear seasonal variations with peaks in July (August) and dominates over the non-AR (AR) storms in the storm-total and the storm-mean *P* during February–July (August–January). The AR storms outnumber the non-AR storms in the heavy-to-extreme *P* ranges. Because large storm *P* can induce high river levels in mountainous basins (Bracken et al., 2008; Pitlick, 1994), the AR (non-AR) storms have a higher potential to induce flooding than the non-AR (AR) storms in summer (early fall). The AR storms are separated from the non-AR storms in the storm-total and storm-mean *P* beyond the UR for March–September. The UR of the storm-mean *P* is also within the 95% confidence interval for all months except February and December. Because October-February is a dry period, the AR inventory differences may not be critical in determining the effects of ARs on *P*.

The AR storms generate 60% (64%) of the annual (summer) *Q*, similarly, as for *P*. The storm-total and the storm-mean *Q* of the AR (non-AR) storms exhibit a well-defined annual cycle with peaks during July–August (August–September). The AR storms induce much more extreme *Q* events than the non-AR storms. The *P*-*Q* relationship (Figure 7b) shows that nearly the entire *P* is converted into *Q* for the storms in which *P* exceeds 300 mm storm^{-1}. The URs and 95% confidence intervals of the storm-total and storm-mean *Q* show that the effects of ARs on *Q* can be clearly identified during the wet months. The AR storms generate significantly more storm-total *Q* than the non-AR storms by amounts exceeding the UR in all months from April to September when most of the annual *Q* occurs. The AR inventory differences may not be critical in quantifying the AR effects on the storm-total and storm-mean *Q*. The effects of ARs on the storm-total and storm-mean *P* and *Q* show that ARs play a crucial role in shaping water resources and the occurrence of extreme hydrologic events in the basin.

The annual mean *R* for the basin is 42%, within the range reported in previous studies, with peaks during July–September (Figure 8). The AR storms yield similar monthly storm-total and storm-mean *R* as the non-AR storms throughout the year despite large *P* differences. The separation in the storm-mean *R* between the AR- and non-AR storms is not clear; the AR storm-mean *R* is within the 95% confidence interval of the non-AR storm-mean *R* for most months. The monthly AR storm-total *R* is generally outside the UR of the non-AR storm-total *R* for most months, although the separation of *R* between the AR and non-AR storms is not as clear as for *P* and *Q*. The UR of the storm-mean *R* is within the 95% confidence interval for all months except December (Figure 8b) for both the AR- and the non-AR storms. Hence, the differences between the AR inventories may not affect the storm-mean *R* of individual storm types although the separation between the AR- and non-AR storm totals are unclear. The lack of significant differences in *R* between the AR and non-AR storms, as well as the phase difference between the annual cycle of *P* and *R*, indicate that *R* is affected not only by *P* but also by other basin-specific parameters.

Previous studies examined key factors that control the response of *Q* to *P* in a basin such as the antecedent SWC (Cao et al., 2020; Detty & McGuire, 2010; Penna et al., 2011; Kim et al., 2019; Merz et al., 2006), catchment areas (Brown et al., 1999; von Freyberg et al., 2014; McGlynn et al., 2004), and *P* characteristics (Blume et al., 2007; Norbiato et al., 2009), among others. Among these factors, the static elements such as the terrain slope and soil texture may be ruled out because *R* follows closely the annual cycle of the storm-total *P*. This implies that the annual cycle of *R* is affected by dynamical hydrologic elements of the basin. Vegetation and SWC may be the two most critical dynamical elements that affect the water budget and undergo clear annual cycles. Vegetation is ruled out as it increases evapotranspiration to decrease *R* in the warm season. The mean SWC over a region including the study basin from the ERA5-Land analysis data (Figure 10) suggests that the response of SWC to *P* can explain the relationship between the annual cycle of *P* and *R*. As a lengthy dry period from October to early June, as well as the period of large transpiration in the growing stage of vegetation, precedes the beginning of the wet season in mid-June, the soils in the basin is driest at the time large *P* starts to occur in June. As much of *P* is absorbed by the dry soil, only a small portion of *P* is converted into *Q*, resulting in a small *R* in June. As high SWC states are reached in late June, a larger fraction of *P* can be converted into *Q* to yield larger *R* in the following wet months, July and August. High SWC is maintained until the end of August by heavy summer rainfall so that a large fraction of *P* can be converted into *R* in September, the month of third largest SWC (Figure 10), to result in a large *R* despite a significant reduction in *P* from August to September. After September, soils become dry again and *R* remains small until the next wet season. Previous observational (Cao et al., 2020) and modeling (Chen

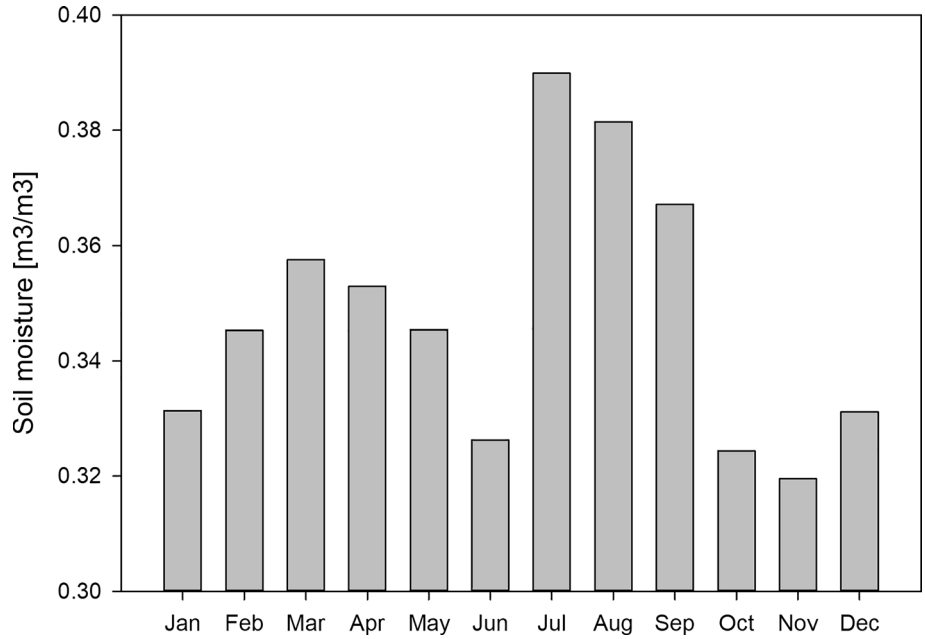

Figure 10. The annual cycle of the root-zone soil moisture in the ERA5-Land (C3S, 2017); available online at: https://cds.climate.copernicus.eu/#1/home.

et al., 2019) studies also showed that the antecedent SWC controls *Q* during AR landfalls in WNA. Quantitative analyses of the detailed water budget for relating the observed *P*, *Q*, and *R* require observed SWC and surface flux data, especially the total evaporation, that are not currently available for this basin.

The AR activity and the impacts of ARs on the basin-scale hydrology in EA found in this study can be particularly useful in the seasonal-to-interannual hydrometeorology forecasting as well as in developing plans for mitigation and adaptation to the impacts of climate change on the water resources and extreme events for southern Korea and similar regions in EA. It would be best to utilize *P* and *Q* for the future period directly for the purposes; however, today's climate models which are practically the sole source of future climate data, lack the skill for reliable simulation of *P* and *Q* because of the deficiencies in the model physics related to precipitation. Observation-based robust relationships between ARs and regional hydrology can be an independent proxy for projecting future *P* characteristics and extreme hydrologic events in conjunction with the simulated water vapor and wind fields because these fields that are used to identify ARs do not suffer directly from the model deficiencies involved in calculating *P*. Because AR characteristics and hydrologic responses to ARs vary following regions, additional studies on the AR-hydrology relationship are warranted for various regions and basins around the world.

Acknowledgments
This work was funded by the Korea Meteorological Administration Research and Development Program "Development of Global Seasonal Forecast System" under Grant (KMA2018-00322), "Development and Assessment of Climate Change Scenario" under Grant (KMA2018-00321), and "Enhancement of Comvergence Technology of Analysis and Forecast on Severe Weather" under Grant (KMA2018-00121). The work by Yoichi Kamae was supported by the Japan Society for the Promotion of Science (JSPS) KAKENHI Grant Number 19H05704. The development of the GW AR inventory was supported by NASA and the California Department of Water Resources.

Data Availability Statement

The GW and PS AR inventories are available in https://ucla.box.com/ARcatalog, and https://agupubs.onlinelibrary.wiley.com/doi/10.1029/2020jd033537 as supporting information, respectively. The KM inventory is available from https://data.mendeley.com/datasets/hnr86n5r36/1.

References

Adams, B. J., Fraser, H. G., Howard, C. D. D., & Sami Hanafy, M. (1986). Meteorological data analysis for drainage system design. *Journal of Environmental Engineering*, *112*(5), 827–848. https://doi.org/10.1061/(ASCE)0733-937210.1061/(asce)0733-9372(1986)112:5(827)

Albano, C. M., Dettinger, M. D., & Harpold, A. A. (2019). Patterns and drivers of atmospheric river precipitation and hydrologic impacts across the western United States. *Journal of Hydrometeorology*, *21*(1), 143–159. https://doi.org/10.1175/JHM-D-19-0119.1

Bartusek, S. T., Seo, H., Ummenhofer, C. C., & Steffen, J. (2021). The role of nearshore air-sea interactions for landfalling atmospheric rivers on the U.S. West Coast. *Geophysical Research Letters*, *48*, e2020GL091388. https://doi.org/10.1029/2020GL091388

Behrangi, A., Guan, B., Neiman, P. J., Schreier, M., & Lambrigtsen, B. (2016). On the quantification of atmospheric rivers precipitation from space: Composite assessments and case studies over the eastern North Pacific Ocean and the western United States. *Journal of Hydrometeorology*, *17*(1), 369–382. https://doi.org/10.1175/JHM-D-15-0061.1

Blamey, R. C., Ramos, A. M., Trigo, R. M., Tomé, R., & Reason, C. J. C. (2018). The Influence of atmospheric rivers over the south Atlantic on winter rainfall in South Africa. *Journal of Hydrometeorology*, *19*(1), 127–142. https://doi.org/10.1175/JHM-D-17-0111.1

Blume, T., Zehe, E., & Bronster, A. (2007). Rainfall—Runoff response, event-based runoff coefficients and hydrograph separation. *Hydrological Sciences Journal*, *52*(5), 843–862. https://doi.org/10.1623/hysj.52.5.843

Bozkurt, D., Sen, O. L., Ezber, Y., Guan, B., Viale, M., & Caglar, F. (2021). Influence of African atmospheric rivers on precipitation and snowmelt in the Near East's highlands. *Journal of Geophysical Research: Atmospheres*, *126*, e2020JD033646. https://doi.org/10.1029/2020JD033646

Bracken, L. J., Cox, N. J., & Shannon, J. (2008). The relationship between rainfall inputs and flood generation in south-east Spain. *Hydrological Processes*, *22*(5), 683–696. https://doi.org/10.1002/hyp.6641

Brown, V. A., McDonnell, J. J., Burns, D. A., & Kendall, C. (1999). The role of event water, a rapid shallow flow component, and catchment size in summer stormflow. *Journal of Hydrology*, *217*(3), 171–190. https://doi.org/10.1016/S0022-1694(98)00247-9

C3S Copernicus Climate Change Service. (2017). *ERA5: Fifth generation of ECMWF atmospheric reanalysis of the global climate. Copernicus Climate Change Service Climate Data Store (CDS).* Retrieved from https://cds.climate.copernicus.eu/#!/home

Cao, Q., Gershunov, A., Shulgina, T., Ralph, F. M., Sun, N., & Lettenmaier, D. P. (2020). Floods due to atmospheric rivers along the U.S. West Coast: The role of antecedent soil moisture in a warming climate. *Journal of Hydrometeorology*, *21*, 1827–1845. https://doi.org/10.1175/jhm-d-19-0242.1

Castro, N. M. D. R., Auzet, A.-V., Chevallier, P., & Leprun, J.-C. (1999). Land use change effects on runoff and erosion from plot to catchment scale on the basaltic plateau of Southern Brazil. *Hydrological Processes*, *13*(11), 1621–1628.

Cerdan, O., Le Bissonnais, Y., Govers, G., Lecomte, V., van Oost, K., Couturier, A., et al. (2004). Scale effect on runoff from experimental plots to catchments in agricultural areas in Normandy. *Journal of Hydrology*, *299*(1), 4–14. https://doi.org/10.1016/j.jhydrol.2004.02.017

Chandimala, J., & Zubair, L. (2007). Predictability of stream flow and rainfall based on ENSO for water resources management in Sri Lanka. *Journal of Hydrology*, *335*(3), 303–312. https://doi.org/10.1016/j.jhydrol.2006.11.024

Chen, X., Leung, L. R., Wigmosta, M., & Richmond, M. (2019). Impact of atmospheric rivers on surface hydrological processes in western U.S. watersheds. *Journal of Geophysical Research*, *124*, 8896–8916. https://doi.org/10.1029/2019jd030468

Conway, D., Persechino, A., Ardoin-Bardin, S., Hamandawana, H., Dieulin, C., & Mahé, G. (2009). Rainfall and water resources variability in sub-saharan Africa during the twentieth century. *Journal of Hydrometeorology*, *10*(1), 41–59. https://doi.org/10.1175/2008JHM1004.1

Corringham, T. W., Ralph, F. M., Gershunov, A., Cayan, D. R., & Talbot, C. A. (2019). Atmospheric rivers drive flood damages in the western United States. *Science Advances*, *5*(12), eaax4631. https://doi.org/10.1126/sciadv.aax4631

Critchley, W. (2013). *Water Harvesting: A manual for the design and construction of water harvesting schemes for plant production [online].* Retrieved from https://www.amazon.com/Water-Harvesting-Construction-Schemes-Production/dp/8172338015

Dee, D. P., Uppala, S. M., Simmons, A. J., Berrisford, P., Poli, P., Kobayashi, S., et al. (2011). The ERA-Interim reanalysis: Configuration and performance of the data assimilation system. *Quarterly Journal of the Royal Meteorological Society*, *137*(656), 553–597. https://doi.org/10.1002/qj.828

Demaria, E. M. C., Dominguez, F., Hu, H., von Glinski, G., Robles, M., Skindlov, J., & Walter, J. (2017). Observed hydrologic impacts of landfalling atmospheric rivers in Salt and Verde River basins of Arizona, United States. *Water Resources Research*, *53*(12), 10025–10042. https://doi.org/10.1002/2017wr020778

Dettinger, M. D., Ralph, F. M., Das, T., Neiman, P. J., & Cayan, D. R. (2011). Atmospheric rivers, floods and the water resources of California. *Water*, *3*(2), 445–478. https://doi.org/10.3390/w3020445

Detty, J. M., & McGuire, K. J. (2010). Threshold changes in storm runoff generation at a till-mantled headwater catchment. *Water Resources Research*, *46*(7). https://doi.org/10.1029/2009WR008102

Esfandiari, N., & Lashkari, H. (2020). Identifying atmospheric river events and their paths into Iran. *Theoretical and Applied Climatology*, *140*(3), 1125–1137. https://doi.org/10.1007/s00704-020-03148-w

Espinoza, V., Waliser, D. E., Guan, B., Lavers, D. A., & Ralph, F. M. (2018). Global analysis of climate change projection effects on atmospheric rivers. *Geophysical Research Letters*, *45*(9), 4299–4308. https://doi.org/10.1029/2017GL076968

Gershunov, A., Shulgina, T., Ralph, F. M., Laver, D. A., & Rutz, J. J. (2017). Assessing the climate-scale variability of atmospheric rivers affecting western North America. *Geophysical Research Letters*, *44*(15), 7900–7908. https://doi.org/10.1002/2017gl074175

Gorodetskaya, I. V., Tsukernik, M., Claes, K., Ralph, F. M., Neff, W. D., & Lipzig, N. P. M. V. (2014). The role of atmospheric rivers in anomalous snow accumulation in East Antarctica. *Geophysical Research Letters*, *41*, 6199–6206. https://doi.org/10.1002/2014GL060881

Gottschalk, L., & Weingartner, R. (1998). Distribution of peak flow derived from a distribution of rainfall volume and runoff coefficient, and a unit hydrograph. *Journal of Hydrology*, *208*(3), 148–162. https://doi.org/10.1016/S0022-1694(98)00152-8

Guan, B., Molotch, N. P., Waliser, D. E., Fetzer, E. J., & Neiman, P. J. (2010). Extreme snowfall events linked to atmospheric rivers and surface air temperature via satellite measurements. *Geophysical Research Letters*, *37*(20), L20401. https://doi.org/10.1029/2010GL044696

Guan, B., & Waliser, D. E. (2015). Detection of atmospheric rivers: Evaluation and application of an algorithm for global studies. *Journal of Geophysical Research: Atmospheres*, *120*(24), 12514–12535. https://doi.org/10.1002/2015JD024257

Guan, B., & Waliser, D. E. (2017). Atmospheric rivers in 20 year weather and climate simulations: A multimodel, global evaluation. *Journal of Geophysical Research: Atmospheres*, *122*, 5556–5581. https://doi.org/10.1002/2016JD026174

Guan, B., & Waliser, D. E. (2019). Tracking atmospheric rivers globally: Spatial distributions and temporal evolution of life cycle characteristics. *Journal of Geophysical Research: Atmospheres*, *124*, 12523–12552. https://doi.org/10.1029/2019JD031205

Guan, B., Waliser, D. E., & Ralph, F. M. (2018). An intercomparison between reanalysis and dropsonde observations of the total water vapor transport in individual atmospheric rivers. *Journal of Hydrometeorology*, *19*, 321–337. https://doi.org/10.1175/JHM-D-17-0114.1

Guan, B., Waliser, D. E., Ralph, F. M., Fetzer, E. J., & Neiman, P. J. (2016). Hydrometeorological characteristics of rain-on-snow events associated with atmospheric rivers. *Geophysical Research Letters*, *43*(6), 2964–2973. https://doi.org/10.1002/2016GL067978

Guo, Y. (2001). Hydrologic design of urban flood control detention ponds. *Journal of Hydrologic Engineering*, *6*(6), 472–479. https://doi.org/10.1061/(ASCE)1084-069910.1061/(asce)1084-0699(2001)6:6(472)

Guo, Y., & Adams, B. J. (1998). Hydrologic analysis of urban catchments with event-based probabilistic models: 1. Runoff volume. *Water Resources Research*, *34*(12), 3421–3431. https://doi.org/10.1029/98WR02449

Guo, Y., & Baetz, B. W. (2007). Sizing of rainwater storage units for green building applications. *Journal of Hydrologic Engineering*, *12*(2), 197–205. https://doi.org/10.1061/(ASCE)1084-069910.1061/(asce)1084-0699(2007)12:2(197)

Guo, Y., Shinoda, T., Guan, B., Waliser, D. E., & Chang, E. K. M. (2020). Statistical relationship between atmospheric rivers and extratropical cyclones and anticyclones. *Journal of Climate*, *33*(18), 7817–7834. https://doi.org/10.1175/JCLI-D-19-0126.1

Hersbach, H., Hersbach, H., Bell, B., Berrisford, P., Hirahara, S., Horányi, A., et al. (2020). The ERA5 global reanalysis. *Quarterly Journal of the Royal Meteorological Society*, *146*, 1999–2049. https://doi.org/10.1002/qj.3803

Hirota, N., Takayabu, Y. N., Kato, M., & Arakane, S. (2016). Roles of an atmospheric river and a cutoff low in the extreme precipitation event in Hiroshima on 19 August 2014. *Monthly Weather Review*, *144*(3), 1145–1160. https://doi.org/10.1175/MWR-D-15-0299.1

Hu, H., Dominguez, F., Wang, Z., Lavers, D. A., Zhang, G., & Ralph, F. M. (2017). Linking atmospheric river hydrological impacts on the U.S. West Coast to Rossby wave breaking. *Journal of Climate*, *30*, 3381–3399. https://doi.org/10.1175/JCLI-D-16-0386.1

Huning, L., Margulis, S., Guan, B., Waliser, D., & Neiman, P. (2017). Implications of detection methods on characterizing atmospheric river contribution to seasonal snowfall across Sierra Nevada, USA, *Geophysical Research Letters*, *44*, 10445–10453. https://doi.org/10.1002/2017GL075201

Huning, L. S., Guan, B., Waliser, D. E., & Lettenmaier, D. P. (2019). Sensitivity of seasonal snowfall attribution to atmospheric rivers and their reanalysis-based detection. *Geophysical Research Letters*, *46*, 794–803. https://doi.org/10.1029/2018GL080783

Ionita, M., Nagavciuc, V., & Guan, B. (2020). Rivers in the sky, flooding on the ground. *Hydrology and Earth System Sciences Discussions*, 1–28. https://doi.org/10.5194/hess-2020-149

Kamae, Y., Mei, W., & Xie, S.-P. (2017). Climatological relationship between warm season atmospheric rivers and heavy rainfall over East Asia. *Journal of the Meteorological Society of Japan. Series II*, *95*(6), 411–431. https://doi.org/10.2151/jmsj.2017-027

Kamae, Y., Mei, W., Xie, S.-P., Naoi, M., & Ueda, H. (2017). Atmospheric rivers over the northwestern Pacific: Climatology and interannual variability. *Journal of Climate*, *30*(15), 5605–5619. https://doi.org/10.1175/JCLI-D-16-0875.1

Kang, J. M., Lee, J., Son, S.-W., Kim, J., & Chen, D. (2018). The rapid intensification of East Asian cyclones around the Korean Peninsula and their surface impacts. *Journal of Geophysical Research*, *125*, e2019JD031632. https://doi.org/10.1029/2019JD031632

Kang, J. M., & Son, S.-W. (2021). Development processes of the East Asian cyclones over the Korean Peninsula. *Weather and Climate Dynamics Discussions*, 1–21. https://doi.org/10.5194/wcd-2020-65

Kim, D., Kim, Y.-O., Jee, H., & Kang, T.-H. (2020). Development of index for flood risk assessment on national scale and future outlook. *Journal of Korea Water Resources Association*, *53*(5), 323–336. https://doi.org/10.3741/JKWRA.2020.53.5.323

Kim, J., Guan, B., Waliser, D. E., Ferraro, R. D., Case, J. L., Iguchi, T., et al. (2018). Winter precipitation characteristics in western US related to atmospheric river landfalls: Observations and model evaluations. *Climate Dynamics*, *50*(1), 231–248. https://doi.org/10.1007/s00382-017-3601-5

Kim, J., Johnson, L., Cifelli, R., Thorstensen, A., & Chandrasekar, V. (2019). Assessment of antecedent moisture condition on flood frequency: An experimental study in Napa River Basin, CA. *Journal of Hydrology: Regional Studies*, *26*, 100629. https://doi.org/10.1016/j.ejrh.2019.100629

Kim, J., Moon, H., Guan, B., Waliser, D. E., Choi, J., Gu, T.-Y., & Byun, Y.-H. (2021). Precipitation characteristics related to atmospheric rivers in East Asia. *International Journal of Climatology*, *41*(S1). https://doi.org/10.1002/joc.6843

Kim, J., Sanjay, J., Mattmann, C., Boustani, M., Ramarao, M. V. S., Krishnan, R., & Waliser, D. (2015). Uncertainties in estimating spatial and interannual variations in precipitation climatology in the India-Tibet region from multiple precipitation datasets. *International Journal of Climatology*, *35*, 4557–4573. https://doi.org/10.1002/joc.4306

Kim, J., Waliser, D. E., Neiman, P. J., Guan, B., Ryoo, J.-M., & Wick, G. A. (2013). Effects of atmospheric river landfalls on the cold season precipitation in California. *Climate Dynamics*, *40*, 465–474. https://doi.org/10.1007/s00382-012-1322-3

Ko, D., Lee, T., & Lee, D. (2018). Spatio-temporal-dependent errors of radar rainfall estimates in flood forecasting for the Nam River Dam basin. *Meteorological Applications*, *25*(2), 322–336. https://doi.org/10.1002/met.1700

Kobayashi, S., Ota, Y., Harada, Y., Ebita, A., Moriya, M., Onda, H., et al. (2015). The JRA-55 reanalysis: General specifications and basic characteristics. *Journal of the Meteorological Society of Japan*, *93*, 5–48. https://doi.org/10.2151/jmsj.2015-001

Konrad, C. P., & Dettinger, M. D. (2017). Flood runoff in relation to water vapor transport by atmospheric rivers over the western United States, 1949–2015. *Geophysical Research Letters*, *44*(22), 456–511. https://doi.org/10.1002/2017GL075399

Lamjiri, M. A., Dettinger, M. D., Ralph, F. M., & Guan, B. (2017). Hourly storm characteristics along the U.S. West Coast: Role of atmospheric rivers in extreme precipitation. *Geophysical Research Letters*, *44*(13), 7020–7028. https://doi.org/10.1002/2017GL074193

Lavers, D. A., Allan, R. P., Wood, E. F., Villarini, G., Brayshaw, D. J., & Wade, A. J. (2011). Winter floods in Britain are connected to atmospheric rivers. *Geophysical Research Letters*, *38*, L23803. https://doi.org/10.1029/2011GL049783

Lavers, D. A., & Villarini, G. (2013a). Atmospheric rivers and flooding over the central United States. *Journal of Climate*, *26*(20), 7829–7836. https://doi.org/10.1175/JCLI-D-13-00212.1

Lavers, D. A., & Villarini, G. (2013b). The nexus between atmospheric rivers and extreme precipitation across Europe. *Geophysical Research Letters*, *40*, 3259–3264. https://doi.org/10.1002/grl.50636

Lavers, D. A., Villarini, G., Allan, R. P., Wood, E. F., & Wade, A. J. (2012). The detection of atmospheric rivers in atmospheric reanalyses and their links to British winter floods and the large-scale climatic circulation. *Journal of Geophysical Research*, *117*(D20), D20106. https://doi.org/10.1029/2012JD018027

Leung, L. R., & Qian, Y. (2009). Atmospheric rivers induced heavy precipitation and flooding in the western U.S. simulated by the WRF regional climate model. *Geophysical Research Letters*, *36*, L03820. https://doi.org/10.1029/2008gl036445

López-Moreno, J. I., Beguería, S., Vicente-Serrano, S. M., & García-Ruiz, J. M. (2007). Influence of the North Atlantic Oscillation on water resources in central Iberia: Precipitation, streamflow anomalies, and reservoir management strategies. *Water Resources Research*, *43*(9), W09411. https://doi.org/10.1029/2007WR005864

Lu, M., Lall, U., Schwartz, A., & Kwon, H. (2013). Precipitation predictability associated with tropical moisture exports and circulation patterns for a major flood in France in 1995. *Water Resources Research*, *49*(10), 6381–6392. https://doi.org/10.1002/wrcr.20512

Mahoney, K., Jackson, D. L., Neiman, P., Hughes, M., Darby, L., Wick, G., et al. (2016). Understanding the role of atmospheric rivers in heavy precipitation in the southeast United States. *Monthly Weather Review*, *144*(4), 1617–1632. https://doi.org/10.1175/MWR-D-15-0279.1

Manda, A., Nakamura, H., Asano, N., Iizuka, S., Miyama, T., Moteki, Q., et al. (2014). Impacts of a warming marginal sea on torrential rainfall organized under the Asian summer monsoon. *Scientific Reports*, *4*(1), 5741. https://doi.org/10.1038/srep05741

Marchi, L., Borga, M., Preciso, E., & Gaume, E. (2010). Characterisation of selected extreme flash floods in Europe and implications for flood risk management. *Journal of Hydrology*, *394*(1), 118–133. https://doi.org/10.1016/j.jhydrol.2010.07.017

Massoud, E., Massoud, T., Guan, B., Sengupta, A., Espinoza, V., De Luna, M., et al. (2020). Atmospheric rivers and precipitation in the Middle East and North Africa (MENA). *Water*, *12*, 2863. https://doi.org/10.3390/w12102863

McGlynn, B. L., McDonnell, J. J., Seibert, J., & Kendall, C. (2004). Scale effects on headwater catchment runoff timing, flow sources, and groundwater-streamflow relations. *Water Resources Research*, *40*(7), W07504. https://doi.org/10.1029/2003WR002494

Merz, R., Blöschl, G., & Parajka, J. (2006). Spatio-temporal variability of event runoff coefficients. *Journal of Hydrology*, *331*(3), 591–604. https://doi.org/10.1016/j.jhydrol.2006.06.008

Mo, R., Brugman, M. M., Milbrandt, J. A., Goosen, J., Geng, Q., Emond, C., et al. (2019). Impacts of hydrometeor drift on orographic precipitation: Two case studies of landfalling atmospheric rivers in British Columbia, Canada. *Weather and Forecasting*, *34*(5), 1211–1237. https://doi.org/10.1175/WAF-D-18-0176.1

Moon, H., Kim, J., Guan, B., Waliser, D. E., Choi, J., Goo, T.-Y., et al. (2019). The effects of atmospheric river landfalls on precipitation and temperature in Korea. *Atmosphere Korean Meteorological Society*, *29*(4), 343–353. https://doi.org/10.14191/Atmos.2019.29.4.343

Moore, B. J., Neiman, P. J., Ralph, F. M., & Barthold, F. E. (2012). Physical processes associated with heavy flooding rainfall in Nashville, Tennessee, and vicinity during 1–2 May 2010: The role of an atmospheric river and mesoscale convective systems. *Monthly Weather Review*, *140*(2), 358–378. https://doi.org/10.1175/MWR-D-11-00126.1

Mundhenk, B. D., Barnes, E. A., & Maloney, E. D. (2016). All-season climatology and variability of atmospheric river frequencies over the North Pacific. *Journal of Climate*, *29*(13), 4885–4903. https://doi.org/10.1175/JCLI-D-15-0655.1

Nash, D., Waliser, D., Guan, B., Ye, H., & Ralph, M. (2018). The role of atmospheric rivers in extratropical and polar hydroclimate. *Journal of Geophysical Research: Atmospheres*, *123*, 6804–6821. https://doi.org/10.1029/2017JD028130

Neiman, P. J., Ralph, F. M., Wick, G. A., Lundquist, J. D., & Dettinger, M. D. (2008). Meteorological characteristics and overland precipitation impacts of atmospheric rivers affecting the west coast of north America based on eight years of SSM/I satellite observations. *Journal of Hydrometeorology*, *9*(1), 22–47. https://doi.org/10.1175/2007JHM855.1

Neiman, P. J., Schick, L. J., Ralph, F. M., Hughes, M., & Wick, G. A. (2011). Flooding in western Washington: The connection to atmospheric rivers. *Journal of Hydrometeorology*, *12*(6), 1337–1358. https://doi.org/10.1175/2011JHM1358.1

Norbiato, D., Borga, M., Merz, R., Blöschl, G., & Carton, A. (2009). Controls on event runoff coefficients in the eastern Italian Alps. *Journal of Hydrology*, *375*(3), 312–325. https://doi.org/10.1016/j.jhydrol.2009.06.044

Paltan, H., Waliser, D., Lim, W. H., Guan, B., Yamazaki, D., Pant, R., & Dadson, S. (2017). Global floods and water availability driven by atmospheric rivers. *Geophysical Research Letters*, *44*(20), 387–410. https://doi.org/10.1002/2017GL074882

Park, C., Son, S.-W., & Kim, H. (2021a). Distinct features of atmospheric rivers in the early versus late East Asian summer monsoon and their impacts on monsoon rainfall. *Journal of Geophysical Research*, *126*, e2020JD033537. https://doi.org/10.1029/2020JD033537

Park, C., Son, S.-W., & Kim, J.-H. (2021b). Role of baroclinic trough in triggering vertical motion during summertime heavy rainfall events in Korea. *Journal of the Atmospheric Sciences*. https://doi.org/10.1175/jas-d-20-0216.1

Park, J. I., & Singh, V. P. (1996). Temporal and spatial characteristics of rainfall in the Nam river dam basin of Korea. *Hydrological Processes*, *10*, 1155–1171.

Penna, D., Tromp-van Meerveld, H. J., Gobbi, A., Borga, M., & Dalla Fontana, G. (2011). The influence of soil moisture on threshold runoff generation processes in an alpine headwater catchment. *Hydrology and Earth System Sciences*, *15*(3), 689–702. https://doi.org/10.5194/hess-15-689-2011

Pitlick, J. (1994). Relation between peak flows, precipitation, and physiography for five mountainous regions in the western USA. *Journal of Hydrology*, *158*(3), 219–240. https://doi.org/10.1016/0022-1694(94)90055-8

Ralph, F. M., Neiman, P. J., & Wick, G. A. (2004). Satellite and CALJET aircraft observations of atmospheric rivers over the eastern North Pacific Ocean during the winter of 1997/98. *Monthly Weather Review*, *132*(7), 1721–1745. https://doi.org/10.1175/1520-0493(2004)132<1721:SACAOO>2.0.CO;2

Ralph, F. M., Neiman, P. J., Wick, G. A., Gutman, S. I., Dettinger, M. D., Cayan, D. R., & White, A. B. (2006). Flooding on California's Russian river: Role of atmospheric rivers. *Geophysical Research Letters*, *33*(13), L13801. https://doi.org/10.1029/2006GL026689

Ralph, F. M., Wilson, A. M., Shulgina, T., Kawzenuk, B., Sellars, S., Rutz, J. J., et al. (2019). ARTMIP-early start comparison of atmospheric river detection tools: How many atmospheric rivers hit northern California's Russian River watershed? *Climate Dynamics*, *52*, 4973–4994. https://doi.org/10.1007/s00382-018-4427-5

Ramos, A. M., Martins, M. J., Tomé, R., & Trigo, R. M. (2018). Extreme precipitation events in summer in the Iberian Peninsula and its relationship with atmospheric rivers. *Frontiers of Earth Science*, *6*. https://doi.org/10.3389/feart.2018.00110

Ramos, A. M., Trigo, R. M., Liberato, M. L. R., & Tomé, R. (2015). Daily precipitation extreme events in the Iberian Peninsula and its association with atmospheric rivers. *Journal of Hydrometeorology*, *16*(2), 579–597. https://doi.org/10.1175/JHM-D-14-0103.1

Rodríguez-Blanco, M. L., Taboada-Castro, M. M., & Taboada-Castro, M. T. (2012). Rainfall-runoff response and event-based runoff coefficients in a humid area (northwest Spain). *Hydrological Sciences Journal*, *57*(3), 445–459. https://doi.org/10.1080/02626667.2012.666351

Rutz, J. J., Guan, B., Bozkurt, D., Gorodetskaya, I., Gershunov, A., Lavers, D. A., et al. (2020). Global and regional perspectives. In F. M. Ralph, M. D. Dettinger, J. J. Rutz, & D. E. Waliser (Eds.), *Atmospheric rivers* (pp. 89–140). Springer. https://doi.org/10.1007/978-3-030-28906-5_4

Rutz, J. J., Shields, C. A., Lora, J. M., Payne, A. E., Guan, B., Ullrich, P., et al. (2019). The atmospheric river tracking method intercomparison project (ARTMIP): Quantifying uncertainties in atmospheric river climatology. *Journal of Geophysical Research: Atmospheres*, *124*(24), 13777–13802. https://doi.org/10.1029/2019JD030936

Ryu, Y., Lim, Y.-J., Ji, H.-S., Park, H.-H., Chang, E.-C., & Kim, B.-J. (2017). Applying a coupled hydrometeorological simulation system to flash flood forecasting over the Korean Peninsula. *Asia-Pacific Journal of Atmospheric Sciences*, *53*(4), 421–430. https://doi.org/10.1007/s13143-017-0045-0

Schneider, P., Lippmann-Pipke, J., & Schoenherr, J. (2005). *Quality assurance of water balance simulations at the landfill cover test fields Bautzen/Nadelwitz, Germany. Dimensioning landfill surface liner systems using water balance models proceedings* (pp. 91–106).

Sharma, A. R., & Dery, S. J. (2020a). Contribution of atmospheric rivers to annual, seasonal, and extreme precipitation across British Columbia and southeastern Alaska. *Journal of Geophysical Research*, *124*, 13777–13802. https://doi.org/10.1029/2019jd031823

Sharma, A. R., & Déry, S. J. (2020b). Variability and trends of landfalling atmospheric rivers along the Pacific Coast of northwestern North America. *International Journal of Climatology*, *40*(1), 544–558. https://doi.org/10.1002/joc.6227

Sherman (1932). Streamflow from rainfall by the unit-graph method. *Engineering News Record*, *108*, 501–505.

Shields, C. A., Leung, L.-Y., Ralph, F. M., Wehner, M., Kawzenuk, B., Lora, J. M., et al. (2018). Atmospheric river tracking method intercomparison project (ARTMIP): Project goals and experimental design. *Geoscientific Model Development*, *11*, 2455–2474. https://doi.org/10.5194/gmd-11-2455-2018

Sivapalan, M., Blöschl, G., Merz, R., & Gutknecht, D. (2005). Linking flood frequency to long-term water balance: Incorporating effects of seasonality. *Water Resources Research*, *41*(6), W06012. https://doi.org/10.1029/2004WR003439

Slinskey, E. A., Loikith, P. C., Waliser, D. E., Guan, B., & Martin, A. (2020). A climatology of atmospheric rivers and associated precipitation for the seven U.S. National Climate Assessment regions. *Journal of Hydrometeorology*, *21*, 2439–2456. https://doi.org/10.1175/JHM-D-20-0039.1

Stohl, A., Forster, C., & Sodemann, H. (2008). Remote sources of water vapor forming precipitation on the Norwegian west coast at 60°N—A tale of hurricanes and an atmospheric river. *Journal of Geophysical Research*, *113*(D5), D05102. https://doi.org/10.1029/2007JD009006

Trenberth, K. E., & Stepaniak, D. P. (2003). Seamless poleward atmospheric energy transports and implications for the Hadley circulation. *Journal of Climate*, *16*(22), 3706–3722. https://doi.org/10.1175/1520-0442(2003)016<3706:SPAETA>2.0.CO;2

Trigo, R. M., Pozo-Vázquez, D., Osborn, T. J., Castro-Díez, Y., Gámiz-Fortis, S., & Esteban-Parra, M. J. (2004). North Atlantic oscillation influence on precipitation, river flow and water resources in the Iberian Peninsula. *International Journal of Climatology*, *24*(8), 925–944. https://doi.org/10.1002/joc.1048

Viale, M., Valenzuela, R., Garreaud, R. D., & Ralph, F. M. (2018). Impacts of atmospheric rivers on precipitation in southern South America. *Journal of Hydrometeorology*, *19*(10), 1671–1687. https://doi.org/10.1175/JHM-D-18-0006.1

von Freyberg, J., Radny, D., Gall, H. E., & Schirmer, M. (2014). Implications of hydrologic connectivity between hillslopes and riparian zones on streamflow composition. *Journal of Contaminant Hydrology*, *169*, 62–74. https://doi.org/10.1016/j.jconhyd.2014.07.005

von Freyberg, J., Studer, B., Rinderer, M., & Kirchner, J. W. (2018). Studying catchment storm response using event- and pre-event water volumes as fractions of precipitation rather than discharge. *Hydrology and Earth System Sciences*, *22*(11), 5847–5865. https://doi.org/10.5194/hess-22-5847-2018

Waliser, D., & Guan, B. (2017). Extreme winds and precipitation during landfall of atmospheric rivers. *Nature Geoscience*, *10*(3), 179–183. https://doi.org/10.1038/ngeo2894/

Ye, C., Zhang, H., Moise, A., & Mo, R. (2020). Atmospheric rivers in the Australia-Asian region: A BoM-CMA collaborative study. *Journal of Southern Hemisphere Earth Systems Science*, *70*, 3. https://doi.org/10.1071/ES19025

Young, A. M., Skelly, K. T., & Cordeira, J. M. (2017). High-impact hydrologic events and atmospheric rivers in California: An investigation using the NCEI storm events database. *Geophysical Research Letters*, *44*(7), 3393–3401. https://doi.org/10.1002/2017GL073077

Zhang, Z., Ralph, F. M., & Zheng, M. (2019). The relationship between extratropical cyclone strength and atmospheric river intensity and position. *Geophysical Research Letters*, *46*(3), 1814–1823. https://doi.org/10.1029/2018GL079071

Zhu, Y., & Newell, R. E. (1998). A proposed algorithm for moisture fluxes from atmospheric rivers. *Monthly Weather Review*, *126*(3), 725–735. https://doi.org/10.1175/1520-0493(1998)126<0725:apafmf>2.0.co;2

Erratum

In the originally published article, Figure 8 was incorrect. The figure has been updated and this may be considered the authoritative version of record.